JACS
JOURNAL OF THE AMERICAN CHEMICAL SOCIETY

Article

pubs.acs.org/JACS

Coordination Chemistry and Antisolvent Strategy to Rare-Earth Solid Solution Colloidal Spheres

Cheng Chao Li and Hua Chun Zeng*

Department of Chemical and Biomolecular Engineering, Faculty of Engineering, National University of Singapore, 10 Kent Ridge Crescent, Singapore 119260

Supporting Information

ABSTRACT: We have devised in this work a general synthetic strategy for preparation of single- and multicomponent rare-earth coordination polymer colloidal spheres (RE-CPCSs). This strategy is based on an integration of coordination chemistry and antisolvent effect for synchronized precipitation. Highly monodisperse RE-CPCSs with homogeneous mixing of RE elements, which are not readily attainable by any existing methods, have been successfully prepared for the first time. In addition, the type and molar ratio of these colloidal spheres can be adjusted easily in accordance to the variety and dosage of precursor salts. The molar ratio of RE elements in as-prepared colloidal spheres shows a linear relationship to that of starting reactants. Furthermore, the RE-based core/shell colloidal spheres can be facilely prepared by introducing other metal salts (beyond lanthanide elements) owing to their different coordination chemistry and precipitation behavior. By adjusting concentrations of the ionic activators, luminescent properties can be tuned accordingly. Moreover, the RE-CPCSs can be transformed to monodisperse lanthanide oxide spheres via simple heat treatment. We believe that the present synthetic strategy provides a viable route to prepare other lanthanide-containing colloidal spheres that have enormous potential for future applications as optoelectronic devices, catalysts, gas sensors, and solar cells.

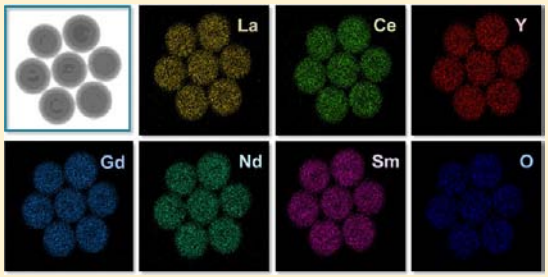

INTRODUCTION

Colloidal spheres have been frequently studied in the context of materials science, physics, chemistry, and biology because of their widespread applications, such as photonics, drug delivery, heterogeneous catalysis, combinatorial synthesis, biolabeling, and chemical and optical sensing.[1−5] Monodisperse colloidal spheres may also be considered as fundamental building blocks for the fabrication of devices due to their spherical geometry and narrow size distribution.[6−11] Thanks to many years of continuous efforts, the scope of colloidal materials has been rapidly broadened as the number of synthetic strategies for semiconductor and metal colloidal spheres increases.[12−20] At present, research efforts in this field mainly focus on the design and synthesis of multicomponent hybrid colloidal particles that integrate several functionalities into one single particle for targeted applications.[21−28] Moreover, controlled combination of different components can greatly improve overall performance of colloidal particles and even lead to unprecedented findings, such as synergistic effects.[29−31] For instance, coupling rare-earth (RE) metal ions with metal nanomaterials has been widely investigated to enhance the light luminescence of lanthanides.[32] The photoluminescent properties of the RE materials are significantly affected by the near-field electrodynamical environment, which depends sensitively on the distance between the material and the metal surface.

RE colloidal sphere is one of the most important colloidal materials across a variety of applications, such as phosphors, solar cells, biomarkers, and catalysts.[33,34] Particularly, multicomponent RE colloidal spheres have gained considerable attention in recent years because of their potential to replace conventional lighting sources in optical devices and three-dimensional backlighting for color displays.[35,36] In addition, multifunctional colloidal spheres achieved by combination of two or more kinds of RE elements are expected to provide more simultaneous detections for biomedical probes compared to conventional biolabeling.[37] The success of RE colloidal spheres in these applications relies largely on the availability of RE colloidal spheres with controlled composition, dispersibility, particle size, and elemental distribution. To this end, many synthetic routes, such as spray pyrolysis, sol−gel process, and urea precipitation, have been developed.[38−40] Despite this great advancement, however, there still exists many intractable problems that hinder the development of this field, such as hollow/porous morphology and wide particle size distribution. Even though the urea-based homogeneous precipitation (UBHP) technique developed by Matijevic et al. more than two decades ago has been successful in fabricating monodisperse colloidal spheres of single-component lanthanides, it is very hard to extend this technique to multicomponent RE systems.[41] They found that light lanthanides tend to precipitate in a way different from those heavier ones in terms of the morphology of resultant particles. Besides, lanthanide dopants are not homogeneously distributed within individual particles

Received: July 24, 2012
Published: October 23, 2012

   dx.doi.org/10.1021/ja307280v | J. Am. Chem. Soc. 2012, 134, 19084−19091

due to their essential differences in physicochemical properties, such as solubility product constant and ionic radius (i.e.; the lanthanide contraction phenomenon). Such local concentration gradients within each particle would result in concentration quenching of luminescence and thus a poorer luminescent performance.

Herein, we report a general synthetic strategy to prepare single and multicomponent RE coordination polymer colloidal spheres (RE-CPCSs) with a uniform size distribution and elemental mixing. Different from the traditional UBHP route, our strategy is based on coordination chemistry, and it provides a new mixing mechanism to realize homogeneous distribution of each element within spheres. An array of binary, ternary, and even senary RE colloidal spheres has been successfully synthesized. The type and composition of these RE-CPCSs can be further tailor made. In particular, molar ratio of RE elements in the product spheres shows a linear relationship with their starting chemicals and the resultant RE-CPCSs exhibit tunable luminescent properties with varying concentration of the included lanthanide activators. On the basis of this strategy, we have also developed new synthetic methods for the preparation of unitary and multinary as well as core/shell lanthanide oxides from their corresponding solid precursors RE-CPCSs.

EXPERIMENTAL SECTION

Synthesis of RE-CPCSs. In a typical synthesis, 0.25 mmol of RE nitrate hydrate (RE = La, Ce, Y, Nd, Sm, Gd, Er, Yb; Supporting Information SI-1) was dissolved in glycols (EG or DEG, 5 mL) under vigorous stirring, followed by addition of 2 mL of concentrated nitric acid (69%). Afterward, 35 mL of acetone was added to form a clear solution. The resultant mixture was stirred for another 30 min and then transferred to a Teflon-lined stainless steel autoclave (volume capacity 50 mL), which was heated to 100 °C and maintained at this temperature for 10 h. The unitary RE-CPCSs were harvested by centrifugation, washed with ethanol three times, and dried at 60 °C in an electric oven for further usage. The multicomponent RE colloidal spheres were solvothermally prepared with a manner similar to that for single component colloidal spheres as stated above. The total concentration of RE nitrate was kept constant at 0.30 mmol.

Synthesis of Al@RE Core/Shell Colloidal Spheres. Into diethylene glycol (DEG, 5 mL), 0.25 mmol of aluminum isopropoxide and 0.25 mmol of RE nitrate hydrate (RE = La, Ce, Y, Nd, Sm, Gd, Er, Yb) were added. Two mL of concentrated nitric acid was then added to make aluminum isopropoxide dissolve under vigorous stirring. After 10 min, 35 mL of acetone was added into the above solution. The resultant mixture was then transferred to a Teflon-lined autoclave and kept inside an electric oven at 100 °C for 10 h. The product was collected and washed several times with water and ethanol. To tune the component and content of shell, two or more kinds of RE nitrate salts were introduced into the above reaction system. The total concentration of RE nitrates was kept constant at 0.30 mmol.

Synthesis of Bi@RE and Al@Bi/RE Core/Shell Colloidal Spheres. All experimental conditions for synthesis of Bi@RE core/shell colloidal spheres were kept the same with those used in the preparation of Al@RE core/shell colloidal spheres, and only the corresponding precursor salts were replaced with 0.125 mmol of bismuth acetate. To prepare Al@Bi/RE core/double-shell colloidal spheres, three metal precursors (bismuth acetate, aluminum isopropoxide, and RE nitrate hydrate) were added into the reaction system at the same time.

Synthesis of Single and Multicomponent and Core/Shell RE Oxide Colloidal Spheres. In laboratory air, the above prepared single component, multicomponent, and core/shell RE-CPCSs were dried first at 60 °C in an electric oven and then converted to corresponding RE oxides by thermal decomposition at 500−800 °C for 4 h in an electric furnace with static air.

Characterization. Crystallographic phases of the prepared products were investigated by X-ray power diffraction method (XRD) using Bruker D8 Advance with Cu K_α radiation. Morphology and compositional investigations with transmission electron microscopy (TEM) and energy dispersive X-ray spectroscopy (EDX) were carried out on JEM-2010 and JEM-2100F (JEOL) instruments, operated with an electron kinetic energy of 200 kV. Fourier-transform infrared (FTIR) spectra of RE coordination polymer colloidal spheres were recorded with KBr pellet technique using a Bio-Rad FTS-135 FTIR spectrometer. Thermogravimetric analysis and differential thermal analysis (TGA-DTA; Shimadzu DTG-60 AH) was also performed to determine organic component of the samples at a heating rate of 10 °C/min from 50 to 800 °C with an air flow rate of 100 mL/min. The chemical components RE-CPCSs were analyzed by liquid chromatography mass spectrometry (LC-MS, Bruker amaZonX) coupled with an Agilent Poroshell 120 SB-C18 column. The mean diameter and diameter distribution of colloidal spheres in this work were measured by the Brook Heaven 200-SM laser light scattering instrument. The content of carbon, hydrogen, and nitrogen were determined by Elementar Vario Micro Cube.

Gas Sensing Measurement. The obtained RE oxide products were mixed with ethanol and hand ground in an agate mortar to form slurries mixture and then laid uniformly onto the surface of the ceramic tubes of the sensors, on which two platinum electrodes were already printed. The fabricated sensors were annealed at 300 °C for 2 h in a muffle furnace and then connected in series with a standard resistor. Before the sensing test, an aging process was performed in laboratory air until the resistance of the sensor was stable. In a typical ethanol-sensing measurement, a certain volume of liquid ethanol was injected into a gas chamber. The concentration of ethanol was calculated with an assumption that all the ethanol would be gasified. Under a bias of 5 V, the sensors were put into/taken out from the gas chamber installed with ethanol vapor. The resistance response of the sensor for the test gas was measured by monitoring the voltage across the load resistor.

RESULTS AND DISCUSSION

The notable differences in solubility product constant, ionic radius, saturated concentration and growth rate in the precipitation reaction are the main factors that hinder the preparation of multicomponent colloidal particles of lanthanides with a narrow size distribution and even elemental distribution. Therefore, it is difficult to exercise the control over the precipitation behavior of participating RE element with conventional preparation methods. Hence, it is important to devise a newer synthetic strategy based on general physical or chemical properties of all lanthanide ions. Ideally, under such a synthetic condition, all RE ions would share the same precipitation step, and thus uniform multicomponent RE products could be made. Thinking along this line, we found that the common coordination properties of RE ions with organic ligands actually offer us such a possibility. The lanthanides, a large unique group of metal elements, are located at the same position in the periodic table. In particular, their *f* electronic configurations and large ionic radii render a similar environment for coordination binding, though their ionic radii are different due to lanthanide contraction. Thus, ligand dependency of this group of elements is relatively insignificant. On the other hand, considering possible synchronized precipitation for these metal ions, the antisolvent effect of acetone has been proven to be efficient to achieve shape control of the precipitate from phase separation.[42] Due to its low dielectric constant and good miscibility with most organic solvents, acetone can decrease drastically the solubility of a reaction product from its existing solvent. Under such conditions, reaction products will segregate from a solution

dx.doi.org/10.1021/ja307280v | J. Am. Chem. Soc. 2012, 134, 19084−19091

phase to form a spherical morphology owing to energy minimization of the system. Furthermore, the dielectric constant of a mixed solvent greatly affects the energy barrier between two particles, according to DLVO theory,[43] which inhibits agglomeration. In our present study, the volume ratio between DEG and acetone was optimized at 1:7. This synthetic route is versatile and effective for the preparation of RE-CPCSs. Figure 1 shows some representative TEM images of the RE-

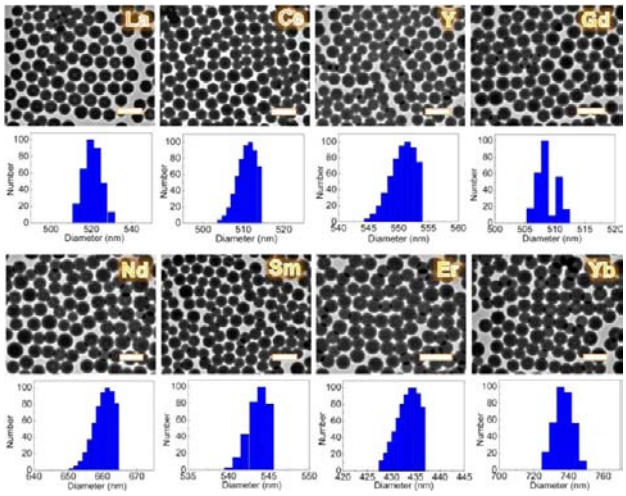

Figure 1. Typical TEM images and LLS size-distribution diagrams of the as-obtained unitary RE-CPCSs. All scale bars: 1 μm.

CPCSs with La, Ce, Y, Gd, Nd, Sm, Er, and Yb, elucidating that synthesis of monodisperse colloidal spheres in a large quantity has been realized. Consistent with the TEM observation, laser light scattering (LLS) technique (Figure 1) further determines that the hydrodynamic diameters of these well-dispersed spheres are in the range of 400−700 nm, and they are indeed stable in solution. In order to demonstrate the effectiveness of this chemical route, a total of six lanthanide salts, such as lanthanum, cerium, yttrium, gadolinium, neodymium, and samarium nitrates, were randomly chosen in our preparation. Figure 2a shows the TEM images of this senary product, and

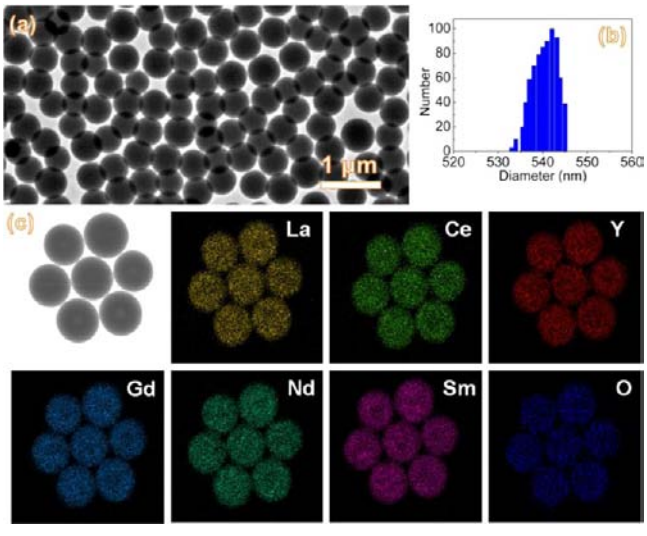

Figure 2. (a) Typical TEM images, (b) LLS size distribution diagram, and (c) elemental mappings of senary RE-CPCSs.

once again, uniform spherical morphology and small size distribution of the particles are evident. Using the LLS technique, the average diameter of these RE-CPCSs was found to be ca. 540 nm (Figure 2b). No noticeable difference is found between the TEM images of multinary and unitary RE-CPCSs. The corresponding chemical mappings are also displayed in Figure 2. As can be seen, all elemental components are evenly distributed within the spheres. An energy dispersive X-ray spectroscopy (EDX) analysis further reveals the existence of all six lanthanide elements La, Ce, Y, Gd, Nd, and Sm (SI-2). The molar ratios of each element in the final RE-CPCSs are approximately equal to the initial ratios of the nitrate salts (SI-2). Not surprisingly, binary or ternary RE-CPCSs can also be obtained simply by mixing two or three types of precursor salts. A series of binary or ternary RE-CPCSs has been thus prepared; all of them show a uniform spherical morphology and homogeneous metal distribution (SI-3). Importantly, these RE-CPCSs can be designed and synthesized with high precision. The molar ratio of each lanthanide element in the final colloidal spheres can be tuned facilely in accordance to the preset ratio of metal precursors, and a linear relationship between them is found from this work (SI-4).

To understand the chemical-bonding situation in the colloidal products, FTIR spectroscopy was employed in our study. In our FTIR spectra of RE-CPCSs (SI-5), a broad absorption band centered at ~3450 cm^{-1} is attributed to O−H stretching vibration of hydrogen-bonded hydroxyl groups in glycols and adsorbed water, while the peaks at around 1630 cm^{-1} can be assigned to the asymmetric stretching vibrations of O−C═O.[44] Furthermore, the bands at 1070 cm^{-1} are attributed to the stretching vibrations of C−O bond, and the bands at ca. 1308 cm^{-1} to the C−H bending vibrations. Other peaks at 790 and 500 cm^{-1} present in all these samples can be ascribed to the chelating carboxylate oxygen to a metal center. Altogether, IR absorptions of O−H, C−H, and C−O−C species indicate the existence of glycol derivatives in the RE-CPCSs. Besides, X-ray diffraction (XRD) patterns reveal the amorphous nature of these spheres (SI-6). Such a matter state should be beneficial to the ionic mixing in these multi-component RE-CPCSs, because the lattice matching is crucial for the preparation of multicomponent crystalline particles. The thermal stability and chemical composition of RE-CPCSs have also been investigated with TGA (SI-7). The gradual weight loss before 200 °C is due to the evaporation of trapped products/solvents (e.g., water and DEG). A three-step weight loss is observed at 200−800 °C. The weight loss at about 200−400 °C can be attributed to the dehydration and simultaneous decomposition of organic phase, which are associated with a weak endothermic effect. The fast weight loss started from 400 °C onward is attributable to ignition of organic ligands, accompanied with a strong exothermic event, and the following slope after 400 °C is related to deep oxidation of pyrolysis products to RE oxides.

To shed light on the coordination chemistry involved, several designed experiments were carried out. Scheme 1 summarizes the formation mechanism of RE-CPCSs: (i) glycols were oxidized by nitric acid to form carboxylic derivatives under hydrothermal condition; and (ii) RE ions coordinated with carboxylic derivatives to form colloidal spheres with the help of antisolvent effect. It was found that adding an appropriate amount of nitric acid is essential for the formation of monodisperse RE-CPCSs. In fact, perfect colloidal spheres can only be obtained within a narrow window of acidity. There

dx.doi.org/10.1021/ja307280v | J. Am. Chem. Soc. 2012, 134, 19084−19091

Scheme 1. Schematic Illustration of the Synthesis of RE-CPCSs and Their Transformation into Corresponding RE Oxides: (i) Formation of Ligands by Oxidation of Glycols under Hydrothermal Conditions; and (ii) Coordination Precipitation of RE Ions with the Help of Antisolvent Effects[a]

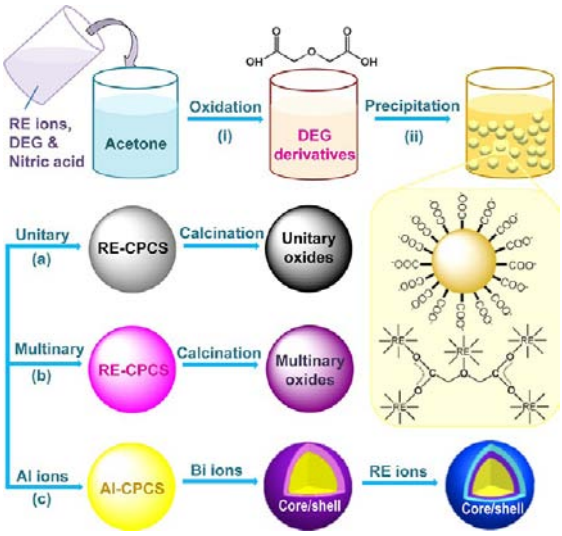

[a]With addition of different precursor salts, the unitary (a), multinary (b), and core/shell RE-CPCSs (c), and RE oxide spheres can be easily prepared accordingly.

are two major roles that nitric acid plays in the synthesis. First, a large amount of nitric acid present in the solution resulted in a low pH value in the initial mixed reaction solution, which greatly inhibited coordination precipitation of RE ions, since the product RE-CPCSs could also be easily dissolved in an initial reaction solution. Further consumption of nitric acid in the solution leads to a slow increase in the pH value of reaction solution. A pH analysis of the reaction solution indicates that nearly 93% nitric acid was consumed after 10 h of reaction (SI-8). As the pH value increased, RE coordination polymer nucleate from solution and the RE-CPCSs were then formed through a mechanism analogous to the well-established Stöber method.[16,31] The whole nucleation and growth were controlled by the slow consumption of nitric acid. Second, nitric acid worked as an oxidizing reagent. Though RE elements have a strong coordination effect with oxygen, glycol could not coordinate directly with RE ions to form glycolate products in such a low pH environment. It had to be oxidized into ligand derivatives by this acid during the reaction which then coordinated with lanthanide ions through RE−O bonds (SI-5 and SI-9). The possible oxidation reactions are as follows:

$$\begin{aligned} &HOCH_2CH_2OCH_2CH_2OH \\ &\xrightarrow{\text{hydrolysis}} HOCH_2CH_2OH \\ &\xrightarrow{\text{oxidation}} HOOCCH_2OH \\ &\xrightarrow{\text{oxidation}} HOOCCOOH \\ &\xrightarrow{\text{oxidation}} HCOOH \end{aligned} \quad (1)$$

$$\begin{aligned} &HOCH_2CH_2OCH_2CH_2OH \\ &\xrightarrow{\text{oxidation}} HOOCCH_2OCH_2CH_2OH \\ &\xrightarrow{\text{oxidation}} HOOCCH_2OCH_2COOH \end{aligned} \quad (2)$$

This hypothesis was supported by both LCMS analysis of reaction solution (SI-9) and FTIR study (the appearance of O=C−O group, SI-5).[44] The investigation has been further confirmed by our controlled experiments. Without adding nitric acid in synthesis or by replacing nitric acid with deionized water or other inorganic acids, such as chloride acid or sulfuric acid, not any product could be formed from this reaction, whereas the resultant RE-CPCSs have a wide size distribution when the amount of concentrated HNO_3 added was insufficient (SI-10). RE elements have a stronger inclination to coordinate with carboxylate groups in comparison with alkoxide groups, which lead to the formation of insoluble RE carboxylates with a high-stability constant. As depicted in SI-9, the main coordination models for RE-CPCSs are bridged coordination with carboxylate groups and single coordination with oxygen atoms from ether (Scheme 1). With these two models, the calculated elemental ratios are in excellent agreement with the CHN results (SI-9).

As mentioned above, the synchronization of precipitation of RE coordination polymers based on the antisolvent effect is the key to achieve uniform distribution of RE elements within each sphere. Conversely, if other metal salts, i.e., beyond RE salts, are also introduced into the synthesis system at the same time, in principle, multicomponent core/shell structures should be attainable with new coordination chemistry involved (Scheme 1). The components, which have lower saturated concentrations and lower pH value requirements for precipitation, would first precipitate and grow into colloidal spheres or cores. With the reaction carried through, the pH value increased gradually, and another component could then grow on the surface of the preformed cores, resulting in biphasic core/shell structures. To validate this postulation, non-RE elements aluminum and bismuth were selected as "impure trivalent ions" to the reaction system while all other experimental conditions were kept identical. The TEM images of Figure 3 indicate that the product spheres have diameters ranging from 500 to 600 nm. The strong contrast between the darker peripheral and the lighter central regions in the TEM image further affirms the core/shell configuration. The sharp interface between the core and the shell indicates a separated nucleation process in the shell growth. Consistent with the TEM results, elemental mapping also reveals the colloidal spheres consist of a core of aluminum and a shell of lanthanum. The formation of core/shell structure can be related to the different saturated concentrations and pH requirements among the different metal ions. In this synthesis, Al^{3+} could first coordinate with glycol derivatives to form aluminum−organic colloidal spheres at a relatively low pH condition (SI-11), followed by La^{3+} ion precipitation (Scheme 1). The latter was a heterogeneous nucleation process requiring lower nucleation energy and saturated concentration in comparison to the homogeneous one. Therefore, with increasing pH value, La^{3+} coordination polymer preferentially grows on the surface of the Al^{3+} coordination polymer colloidal spheres according to the LaMer diagram.[45] Similar to those in the synthesis of multinary RE-CPCSs, moreover, the type and ratio of the component of shell can be adjusted by changing the RE precursor salts. When

dx.doi.org/10.1021/ja307280v | J. Am. Chem. Soc. 2012, 134, 19084−19091

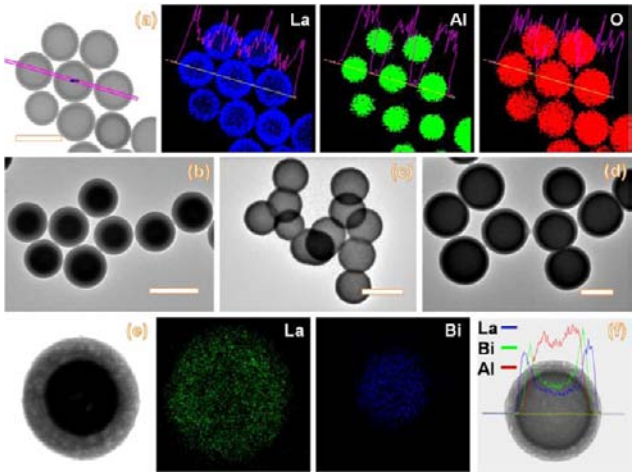

Figure 3. (a) Typical TEM images and elemental mappings of Al@La, (b) Bi@La, and (c) Al@Bi core/shell colloidal spheres, (d) Al@Bi/La core/double-shell colloidal spheres, (e) Bi@La core/shell colloidal sphere and its corresponding elemental mappings, and (f) elemental line-profiles across the Al@Bi/La core/double-shell colloidal sphere probed by EDX technique. All scale bars: 500 nm.

Al^{3+} or Bi^{3+} was added into the reaction system with several kinds of RE nitrate salts, the RE-based core/shell CPCSs with solid solution shells were also prepared. Displayed in Figure 4,

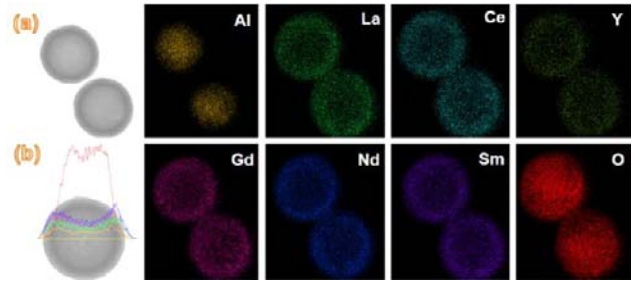

Figure 4. (a) Elemental mappings of Al@6-RE core/shell colloidal spheres and (b) compositional line profile across the nanostructure probed by EDX line scanning.

six RE elements (La, Ce, Y, Gd, Nd, and Sm) are located only in the shell region. It should also be noted that the thickness of the shells could also be controlled by changing the concentration of RE salts (SI-12). The same synthetic strategy can be extended to the general preparation of Al@RE as well as core/shell colloidal spheres with other compositional and structural designs.

Reported in SI-13, a series of such core/shell products was synthesized successfully. By combining different precursor salts, furthermore, core/shell spheres of Al@Bi, Bi@RE, and Al@Bi/RE colloidal spheres could be readily prepared (Figure 3). Thus the nucleation activities can be ranked in the order of Al > Bi > RE.

Using the above-prepared RE-CPCSs as inorganic−organic solid precursors, their chemical transformation can be further pursued. Reported in Figure 5, unitary or multinary RE oxide colloidal spheres have been obtained from thermal decomposition of RE-CPCSs in air atmosphere, as indicated in eq 3. After the heat treatment, the RE oxide spheres retain the similar spherical morphology and size of their parent RE-CPCSs.

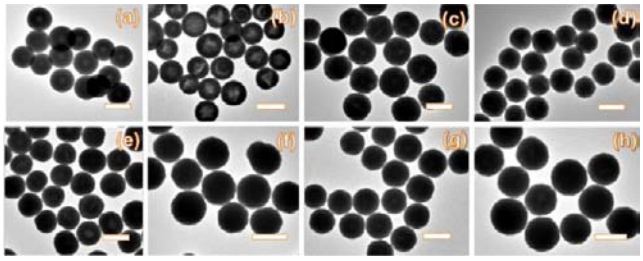

Figure 5. TEM images of RE oxide colloidal spheres obtained by heating their respective solid precursors (RE-CPCSs) at 500 °C for 4 h: (a) La, (b) Ce, (c) Y, (d) Gd, (e) Nd, (f) Sm, (g) Er, and (h) Yb. All scale bars: 500 nm.

$$RE[R(COO)_2]_x \xrightarrow[\Delta]{O_2} RE_2O_2CO_3 \xrightarrow[\Delta]{O_2} RE_2O_3 \quad (3)$$

Our XRD analysis confirms that the RE oxide products are in the expected cubic crystal phase (SI-14). For the multinary RE oxide spheres, as reported in Figure 6, the distribution of each

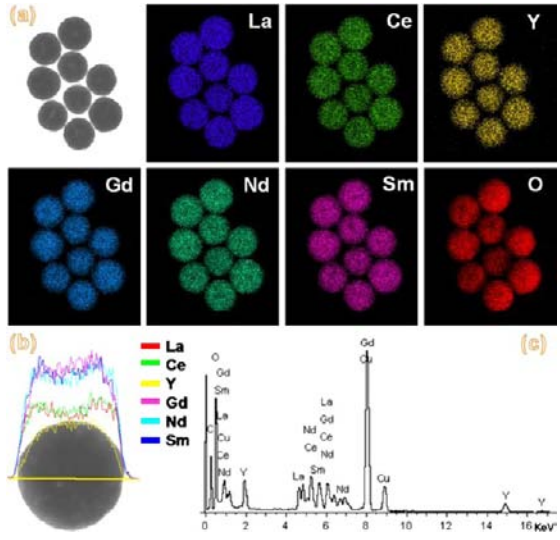

Figure 6. (a) TEM images and elemental mappings of senary RE oxide colloidal spheres obtained by heating their solid precursor (RE-CPCSs) at 500 °C for 4 h; (b) compositional line-profile across a senary RE oxide colloidal sphere probed by EDX technique; and (c) EDX spectrum of senary RE oxide colloidal spheres (La, Ce, Y, Gd, Nd, and Sm).

RE element inside the colloidal spheres is also highly homogeneous even up to a heating temperature of 1000 °C (SI-15). Similarly, the RE oxide core/shell structures could also be generated thermally from their respective parent spheres, as revealed in our TEM investigation displayed in Figure 7 (SI-13), in comparison to their precursors of Figure 3. The compositional line profile shows that the intensities of the RE signal peak at the shell regions, while there is a strong Al signal at the central part (SI-13). However, for the Bi-containing core/shell colloidal spheres, Bi component did not retain the initial shell structure of those in Figure 3f, whereas it melts into irregular particles (Figure 7d). To understand this conversion process, we also conducted a TGA in an air stream. A gradual weight loss was observed up to 800 °C without obvious exothermic process, thereby suggesting different pyrolysis behavior (SI-16), although an in-depth determination of the Bi-containing phase will be needed in the future.

dx.doi.org/10.1021/ja307280v | J. Am. Chem. Soc. 2012, 134, 19084−19091

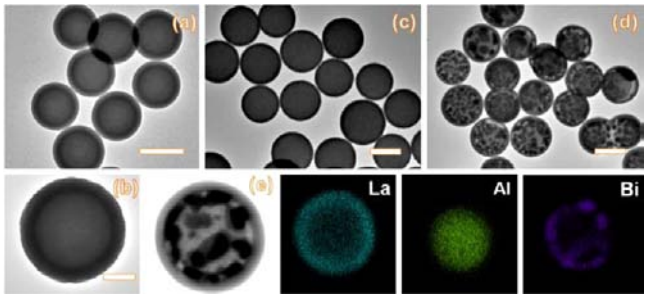

Figure 7. Typical TEM images of RE oxide-based colloidal spheres obtained by heating their respective solid precursors at 500 °C for 4 h: (a,b) Al/La and (c) Al@Bi oxide core/shell spheres, (d,e) Al@Bi/La oxide spheres, and the corresponding element mappings. The scale bar in (d) is 100 nm, and others are 500 nm.

One of the important advantages of these RE colloidal spheres is that they can retain well the unique inherent properties of lanthanide elements. In view of this advantage, our RE-CPCSs are expected to exhibit adjustable combinative properties. In this work, in particular, light-emitting lanthanide ion-doped Gd-based colloidal spheres are designed to achieve monophasic multifunctional bioprobes that present combined magnetic and optical properties within a single particle. To tune photoluminescent properties of Gd-based colloidal spheres, in particular, Eu^{3+} and Tb^{3+} with different relative ratios were introduced into gadolinium coordination polymer host spheres (i.e., Gd-CPCSs). Some emission spectra of the Eu^{3+}- and/or Tb^{3+}-doped Gd-CPCSs under the UV excitation at 241 nm are displayed in Figure 8a. It is found that the pure Eu^{3+}-doped Gd-CPCSs show multiple luminescent properties which comprise two contributions. The characteristic peaks of Eu^{3+} down-conversion emissions at 694, 617, and 592 nm are assigned to the $^5D_0 \rightarrow {}^7F_4$, $^5D_0 \rightarrow {}^7F_2$, and $^5D_0 \rightarrow {}^7F_1$ transitions, respectively.[17,36,46,47] In addition, there is also another wide band from 400 to 550 nm, which is probably related to an intraligand transition.[44] When the Tb^{3+} ions were doped into the Gd-CPCSs, the characteristic emission of Tb^{3+} ions centered at 545 and 491 nm can be observed, besides the Eu^{3+} emissions, which correspond to $^5D_4 \rightarrow {}^7F_5$ and $^5D_4 \rightarrow {}^7F_6$ transitions.[17,48,49]

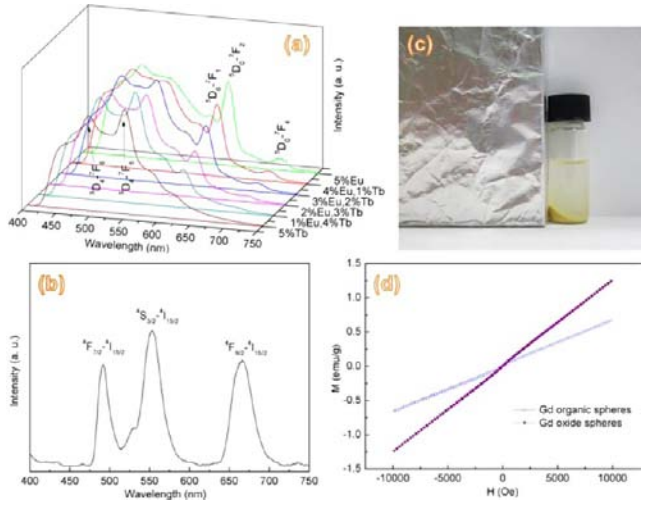

Figure 8. Photoluminescent emission spectra of RE-doped Gd coordination polymer colloidal spheres: (a) Eu and Tb doping under 241 nm UV light excitation, (b) doped with 2% Er and 5% Yb under 980 nm light excitation, (c) magnetic separation of Gd coordination polymer colloidal spheres from solution, and (d) magnetization plots of Gd coordination polymer and Gd oxide colloidal spheres as a function of the applied fields (−10 and 10 kOe) at 300 K.

With increasing concentration of Tb^{3+}, the characteristic emissions of Tb^{3+} ions increase, and those of Eu^{3+} decrease. Finally, pure Tb^{3+}-doped Gd-CPCSs show two wide emission bands centered at 490 and 550 nm. The up-conversion luminescence of the colloidal spheres can also be achieved by the combination of Yb^{3+} and Er^{3+} ions under 980 nm light excitation, as reported in Figure 8b. The emission bands are attributable to transitions within the 4*f*−4*f* levels of Er^{3+}. A dominant red emission originating from the $^4F_{9/2} \rightarrow {}^4I_{15/2}$ transition is observed at 630−680 nm, while the green emissions were observed in the range of 500−580 nm, corresponding to the $^2H_{11/2}/{}^4S_{3/2} \rightarrow {}^4I_{15/2}$ transitions.[44,50] The Gd-CPCSs are magnetically responsive and can be separated conveniently from bulk solution (Figure 8c). Also, Figure 8d gives two magnetization−magnetic field (M−H) plots at 300 K. As the strength of the applied magnetic field increases, the linear correlation between the magnetization and the applied magnetic field indicates typical paramagnetic properties.

In addition to the combinative properties, RE-based solid solutions also hold significant importance in oxidative/reductive catalysis, chemical sensors, and electrolyte materials for fuel cells.[18,51,52] As a salient example, cerium dioxide (CeO_2)-containing solid solution is one of the most well investigated oxides among the RE metal oxides. By itself, CeO_2 has limited applications in these fields because of inadequate thermal stability and oxygen storage under elevated conditions.[53] However, it has been demonstrated that combination with other RE ions to form solid solutions can overcome these drawbacks, thus leading to improved performance. On the other hand, the dopant ions play a key role in modifying the chemical and physical properties of the resultant mixed oxides. For instance, La_2O_3, as a typical basic oxide, is often used to reduce the amount of the acidic sites and result in the formation of Lewis acid−basic pairs on the surface of sensing materials.[54] In ethanol-sensing process, it would be easier for ethanol molecules to be oxidized into CO_2. Under such a circumstance, more electrons are released back to the conduction band, and a higher sensitivity can be achieved. In this way, our RE oxide spheres with tunable composition are thus expected to possess better gas-sensing properties.

Figure 9a presents the ethanol-sensing curves using our RE oxide colloidal spheres at different compositions, which show a typical on and off characteristics. When the sensors are placed in air, some oxygen molecules will adsorb on the surface of these colloidal oxide spheres and capture free electrons in conduction band to form oxygen anionic species (O^-, O^{2-}, and O_2^-), leading to a lower electrical conductance and the sensors stay at an off state. When the sensors are put in the chamber containing ethanol gas, however, the adsorbed oxygen species will react with ethanol molecules, and electrons are released back into the conduction band, resulting in rapid increase in conductance and the sensors are switched on. It should be noted that all the sensors show good stability; no obvious deterioration in sensitivity is observed. As expected, La-containing RE oxides manifest much better sensing properties than the unitary RE oxides (Ce: curve (iii), Y: curve (v), and La: curve (vi)). The sensitivities realized from the La−Ce and La−Y−Ce oxide spheres are 7.1 and 4.1, respectively. However,

dx.doi.org/10.1021/ja307280v | J. Am. Chem. Soc. 2012, 134, 19084−19091

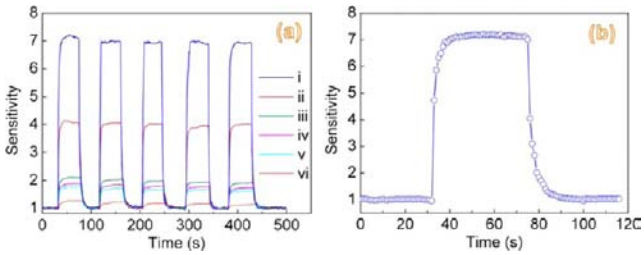

Figure 9. (a) Ethanol-sensing performance (100 ppm) of RE oxide colloidal spheres with different compositions: (i) La–Ce, (ii) La–Y–Ce, (iii) Ce, (iv) Y–Ce, (v) Y, and (vi) La. (b) The enlarged response and recovery process, i.e., (i) La–Ce sample of (a), when exposed to 100 ppm ethanol. The contents of La and Y in all the RE oxides are 10%.

the sensitivities based on unitary RE oxides are only around 2. The improved sensing properties can be attributed to the accelerated oxidation reaction of ethanol molecules after incorporation of La oxide due to the formation of Lewis acid–basic pairs mentioned earlier.[54]

Quite interestingly, the fabricated sensor also exhibits fast response and recovery at a working temperature of 300 °C. The response time of a sensor is defined as the time required for a change in sample resistance to reach 90% of the equilibrium value after the injection of a target gas. Based on this precondition, the calculated response and recovery time of the sensors are only about 5 and 10 s (Figure 9b). Such fast response and recovery can be attributed to the porous nature of individual RE oxide spheres as well as easy access of sensing films formed by the uniform oxide spheres. On an ideal dense packing, uniform spheres can give away ∼26% of the total volume as free void space.[55] The formed pores facilitate the rapid in-and-out diffusion of gas toward the sensing surface. For conventional sensing films formed by particles with different size, additional auxiliary methods are often required to shorten response and recovery time, such as UV illumination and heat treatment.[56,57] However, those methods often cause inconvenience in continuous detection process and sensor fabrication. Therefore, the RE oxide colloidal spheres with tunable compositions (from RE-CPCSs precursors) have been demonstrated to be promising gas-sensing materials apart from their innate photoluminescent properties.

CONCLUSIONS

We have devised in this work a general coordination chemistry-based synthetic strategy to prepare a series of single- and multicomponent monodisperse RE-CPCSs. The type and ratio of the components in the RE-CPCSs can be adjusted in accordance to the variety and amount of precursor salts; the molar ratio of elements in the final colloidal spheres shows a linear relationship to the original reactant ratio. The integration of RE coordination chemistry with antisolvent effect allows synchronized formation of RE-CPCSs with highly mixed RE elements that have not been readily attainable by any existing methods. We have also demonstrated that the prepared RE-CPCSs can be transformed into monodisperse RE oxide spheres by oxidative heating. Apart from Y, La, Ce, Nd, Sm, Eu, Gd, Tb, Er, and Yb that have been demonstrated in this work, in principle, this novel synthetic strategy should also be applicable to the preparation of all RE-containing colloidal spheres which have potential applications across a vast array of technological fields. As an example, we have also applied the RE oxide spheres to sensing application and elucidated promising potential for ethanol detection.

ASSOCIATED CONTENT

Supporting Information

TEM images, element mappings, FTIR spectra, TGA-DTA, XRD, and LC-MS results. This material is available free of charge via the Internet at http://pubs.acs.org.

AUTHOR INFORMATION

Corresponding Author

chezhc@nus.edu.sg

Notes

The authors declare no competing financial interest.

ACKNOWLEDGMENTS

The authors gratefully acknowledge financial supports from the National University of Singapore and GSK Singapore. Thanks are also directed to Professor T. H. Wang's research group at Hunan University, China, for providing the gas-sensing measurements.

REFERENCES

(1) Oh, M.; Mirkin, C. A. *Nature* **2005**, *438*, 651.
(2) Jeong, U.; Wang, Y. L.; Ibisate, M.; Xia, Y. N. *Adv. Funct. Mater.* **2005**, *15*, 1907.
(3) Sun, X. M.; Li, Y. D. *Angew. Chem., Int. Ed.* **2004**, *43*, 597.
(4) Wang, S.; Li, W. C.; Hao, G. P.; Hao, Y.; Sun, Q.; Zhang, X. Q.; Lu, A. H. *J. Am. Chem. Soc.* **2011**, *133*, 15304.
(5) Guo, S. R.; Gong, J. Y.; Jiang, P.; Wu, M.; Lu, Y.; Yu, S. H. *Adv Funct. Mater.* **2008**, *18*, 872.
(6) Li, F.; Josephson, D. P.; Stein, A. *Angew. Chem., Int. Ed.* **2011**, *50*, 360.
(7) Vlasov, Y. A.; Bo, X. Z.; Sturm, J. C.; Norris, D. J. *Nature* **2001**, *414*, 289.
(8) Zhang, J. H.; Li, Y. F.; Zhang, X. M.; Yang, B. *Adv. Mater.* **2010**, *22*, 4249.
(9) Ge, J. P.; Yin, Y. D. *Adv. Mater.* **2008**, *20*, 3485.
(10) Jeong, U.; Xia, Y. N. *Angew. Chem., Int. Ed.* **2005**, *44*, 3099.
(11) Jeong, U.; Kim, J.-U.; Xia, Y. N. *Nano Lett.* **2005**, *5*, 937.
(12) Hu, X. L.; Gong, J. M.; Zhang, L. Z.; Yu, J. C. *Adv. Mater.* **2008**, *20*, 4845.
(13) Li, L.; Tsung, C. K.; Yang, Z.; Stucky, G. D.; Sun, L. D.; Wang, J. F.; Yan, C. H. *Adv. Mater.* **2008**, *20*, 903.
(14) Kelly, T. L.; Yamada, Y.; Che, S. P. Y.; Yano, K.; Wolf, M. O. *Adv. Mater.* **2008**, *20*, 2616.
(15) Bigall, N. C.; Härtling, T.; Klose, M.; Simon, P.; Eng, L. M.; Eychmüller, A. *Nano Lett.* **2008**, *8*, 4588.
(16) Liu, J.; Qiao, S. Z.; Liu, H.; Chen, J.; Orpe, A.; Zhao, D. Y.; Lu, G. Q. *Angew. Chem., Int. Ed.* **2011**, *50*, 5947.
(17) Li, P.; Peng, Q.; Li, Y. D. *Adv. Mater.* **2009**, *21*, 1945.
(18) Liang, X.; Wang, X.; Zhuang, Y.; Xu, B.; Kuang, S. M..; Li, Y. D. *J. Am. Chem. Soc.* **2008**, *130*, 2736.
(19) Wang, D. S.; Xie, T.; Peng, Q.; Li, Y. D. *J. Am. Chem. Soc.* **2008**, *130*, 4016.
(20) Chen, C.; Chen, W.; Lu, J.; Chu, D. R.; Huo, Z. Y.; Peng, Q.; Li, Y. D. *Angew. Chem., Int. Ed.* **2009**, *48*, 4816.
(21) Deng, Y. H.; Cai, Y.; Sun, Z. K.; Liu, J.; Liu, C.; Wei, J.; Li, W.; Liu, C.; Wang, Y.; Zhao, D. Y. *J. Am. Chem. Soc.* **2010**, *132*, 8466.
(22) Deng, Y. H.; Qi, D. W.; Deng, C. H.; Zhang, X. M.; Zhao, D. Y. *J. Am. Chem. Soc.* **2008**, *130*, 28.
(23) Lu, Y.; Zhao, Y.; Yu, L.; Dong, L.; Shi, C.; Hu, M. J.; Xu, Y. J.; Wen, L. P.; Yu, S. H. *Adv. Mater.* **2010**, *22*, 1407.
(24) Yan, X. H.; Li, J. B.; Möhwald, H. *Adv. Mater.* **2012**, *24*, 2663.
(25) Lu, Z. D.; Gao, C. B.; Zhang, Q.; Chi, M. F.; Howe, J. Y.; Yin, Y. D. *Nano Lett.* **2011**, *11*, 3404.

(26) Gao, J. H.; Gu, H. W.; Xu, B. *Acc. Chem. Res.* **2009**, *42*, 1097.
(27) Lee, J. E.; Lee, N.; Kim, T.; Kim, J.; Hyeon, T. *Acc. Chem. Res.* **2011**, *44*, 893.
(28) Lee, J. E.; Lee, N.; Kim, H.; Kim, J.; Choi, S. H.; Kim, J. H.; Kim, T.; Song, I. C.; Park, S. P.; Moon, W. K.; Hyeon, T. *J. Am. Chem. Soc.* **2010**, *132*, 552.
(29) Pang, M. L.; Hu, J. Y.; Zeng, H. C. *J. Am. Chem. Soc.* **2010**, *132*, 10771.
(30) Yao, K. X.; Zeng, H. C. *Chem. Mater.* **2012**, *24*, 140.
(31) Chen, C.; Nan, C. Y.; Wang, D. S.; Su, Q.; Duan, H. H.; Liu, X. W.; Zhang, L. S.; Chu, D. R.; Song, W. G.; Peng, Q.; Li, Y. D. *Angew. Chem., Int. Ed.* **2011**, *50*, 3725.
(32) Zhang, F.; Braun, G. B.; Shi, Y. F.; Zhang, Y. C.; Sun, X. H.; Reich, N. O.; Zhao, D. Y.; Stucky, G. D. *J. Am. Chem. Soc.* **2010**, *132*, 2850.
(33) Liu, J. N.; Bu, W. B.; Zhang, S. J.; Chen, F.; Xing, H. Y.; Pan, L. M.; Zhou, L. P.; Peng, W. J.; Shi, J. L. *Chem.—Eur. J.* **2012**, *18*, 2335.
(34) Bouzigues, C.; Gacoin, T.; Alexandrou, A. *ACS Nano* **2011**, *5*, 8488.
(35) Wakefield, G.; Holland, E.; Dobson, P. J.; Hutchison, J. L. *Adv. Mater.* **2001**, *13*, 1557.
(36) Wang, H.; Yu, M.; Lin, C. K.; Liu, X. M.; Lin, J. *J. Phys. Chem. C* **2007**, *111*, 11223.
(37) Zhou, L. J.; Gu, Z. J.; Liu, X. X.; Yin, W. Y.; Tian, G.; Yan, L.; Jin, S.; Ren, W.; Xing, G. M.; Li, W.; Chang, X. L.; Hu, Z. B.; Zhao, Y. L. *J. Mater. Chem.* **2012**, *22*, 966.
(38) Cho, S. H.; Kwon, S. H.; Yoo, J. S.; Oh, C. W.; Lee, J. D.; Hong, K. J.; Kwon, S. J. *J. Electrochem. Soc.* **2000**, *147*, 3143.
(39) Wang, H.; Lin, C. K.; Liu, X. M.; Lin, J.; Yu, M. *Appl. Phys. Lett.* **2005**, *87*, 181907.
(40) Jing, X.; Ireland, T.; Gibbons, C.; Barber, D. J.; Silver, J.; Vecht, A.; Fern, G.; Trowga, P.; Morton, D. C. *J. Electrochem. Soc.* **1999**, *146*, 4654.
(41) Matijević, E.; Hsu, W. P. *J. Colloid Interface Sci.* **1987**, *118*, 506.
(42) Li, C. C.; Dou, J.; Chen, L. W.; Lin, J. Y.; Zeng, H. C. *ChemCatChem* **2012**, *4*, 1675.
(43) Hunter, R. J. *Foundation of Colloidal Science*; Clarendon Press: Oxford, U.K., 1987, Vol. *1*, p 443.
(44) Gentili, P. L.; Presciutti, F.; Evangelisti, F.; Costantino, F. *Chem.—Eur. J.* **2012**, *18*, 4296.
(45) Zaiser, E. M.; LaMer, V. K. *J. Colloid Interface Sci.* **1948**, *3*, 571.
(46) Luwang, M. N.; Ningthoujam, R. S.; Jagannath, Srivastava, S. K.; Vatsa, R. K. *J. Am. Chem. Soc.* **2010**, *132*, 2759.
(47) Kassab, L. R. P.; Silva, D. S. D.; Almeida, R. D.; Araújo, C. B. D. *Appl. Phys. Lett.* **2009**, *94*, 101912.
(48) Yang, P. P.; Gai, S. L.; Liu, Y. C.; Wang, W. X.; Li, C. X.; Lin, J. *Inorg. Chem.* **2011**, *50*, 2182.
(49) Geng, F. X.; Matsushita, Y.; Ma, R. Z.; Xin, H.; Tanaka, M.; Izumi, F.; Iyi, N.; Sasaki, T. *J. Am. Chem. Soc.* **2008**, *130*, 16344.
(50) Wang, F.; Han, Y.; Lim, C. S.; Lu, Y. H.; Wang, J.; Xu, J.; Chen, H. Y.; Zhang, C.; Hong, M. H.; Liu, X. G. *Nature* **2010**, *463*, 1061.
(51) Li, L. P.; Li, G. S.; Che, Y. L.; Su, W. H. *Chem. Mater.* **2000**, *12*, 2567.
(52) Jasinski, P.; Suzuki, T.; Anderson, H. U. *Sens. Actuators B* **2003**, *95*, 73.
(53) Burbano, M.; Norberg, S. T.; Hull, S.; Eriksson, S. G.; Marrocchelli, D.; Madden, P. A.; Watson, G. W. *Chem. Mater.* **2012**, *24*, 222.
(54) Hieu, N. V.; Kim, H.-R.; Ju, B.-K.; Lee, J.-H. *Sens. Actuators B* **2008**, *133*, 228.
(55) Li, C. C.; Yin, X. M.; Wang, T. H.; Zeng, H. C. *Chem. Mater.* **2009**, *21*, 4984.
(56) Li, J.; Lu, Y. J.; Ye, Q.; Cinke, M.; Han, J.; Meyyappan, M. *Nano Lett.* **2003**, *3*, 929.
(57) Briand, D.; Wingbrant, H.; Sundgren, H.; Schoot, B. V. D.; Ekedahl, L.-G.; Lundström, I.; Rooij, N. F. D. *Sens. Actuators B* **2003**, *93*, 276.

NOTE ADDED AFTER ASAP PUBLICATION

This paper was published ASAP on November 8, 2012. Reference 1 has been updated. The revised version was posted on November 12, 2012.